

GLOBAL FAR-ULTRAVIOLET IMAGE OF THE ERIDANUS SUPERBUBBLE OBSERVED BY FIMS/SPEAR

K. RYU,¹ K. W. MIN,² K.-I. SEON,^{3,4} J. NONESA,² J. EDELSTEIN,⁴ E. KORPELA,⁴ R. SANKRIT,⁴
W. HAN,³ J.-H. PARK,³ AND Y. S. PARK³

Received 2007 November 27; accepted 2008 March 17; published 2008 March 26

ABSTRACT

We present the first far-ultraviolet (FUV; 1350–1750 Å) diffuse emission map of the Eridanus superbubble, obtained using the FIMS/SPEAR instrument. The features seen in the FUV image closely resemble those seen in the H α map, including two prominent arcs identified earlier in H α . While it has been argued that the FUV emission in this region is mostly due to the scattering of star light by dust, a close spectral examination reveals that one of the arcs is abundant in molecules and dust while the other is mainly composed of atomic species. Upon comparison to emission maps in other bands (X-ray, IR, optical H α), we propose the most plausible geometrical structure of this region.

Subject headings: ISM: individual (Eridanus) — ultraviolet: ISM

1. INTRODUCTION

The Eridanus region was first discovered as a 15°-wide extended X-ray “hot spot” (Williamson et al. 1974; Naranan et al. 1976). Heiles (1976) subsequently identified the Eridanus Loop as an expanding shell of H I through a radio survey. Through extensive imaging of the H α emission, Reynolds et al. (1998) and Boumis et al. (2001) revealed large filamentary shell structures in the region. It was suggested that the Eridanus shell was created by one or more supernova explosions in the Orion OB association (Reynolds & Ogden 1979). It is now commonly held that the region contains a large interstellar superbubble, which is maintained by intense stellar winds and ionizing radiation from those stars. A large cavity filled with X-ray-emitting hot gas characterized by *ROSAT* observations (Snowden et al. 1995a) further supports this view. In the FUV band, previous (Murthy et al. 1993) and recent (Kregenow et al. 2006) spectral observations of diffuse emission from the Eridanus Loop revealed that gas at intermediate temperatures ($T \sim 10^5$ K) exists between the hot superbubble interior and the surrounding material.

In this Letter, we present the first FUV diffuse image of the entire Eridanus Loop, obtained with FIMS (Far-ultraviolet Imaging Spectrograph), also known as SPEAR (Spectroscopy of Plasma Emission from Astrophysical Radiation) (Edelstein et al. 2006a). Previous analyses of FIMS/SPEAR data for the Eridanus region focused on spectral features such as H₂ fluorescent and C IV emissions (Ryu et al. 2006; Kregenow et al. 2006). In the present study, we provide new insight into the geometry of the dust and the molecular environment surrounding the superbubble.

2. OBSERVATIONS AND DATA REDUCTION

The Eridanus region was observed with a FIMS/SPEAR instrument on board the Korean satellite *STSAT-1*, which was launched into a 700 km Sun-synchronous orbit on 2003 September 27. FIMS/SPEAR is a dual-channel FUV imaging spectrograph (S channel 900–1150 Å, L channel 1350–1750 Å,

$\Delta\lambda \sim 550$) with large image field of views (S: 4.0° × 4.6', L: 7.5° × 4.3', angular resolution $\sim 10'$) optimized for the observation of diffuse emission. The instrument, mission, and data analysis procedures have been discussed in detail by Edelstein et al. (2006a, 2006b). The region, covering most of the constellations Orion and Eridanus (bounded by $\alpha = 2^{\text{h}}30^{\text{m}}$ to $5^{\text{h}}30^{\text{m}}$ and $\delta = +13^\circ$ to -23° [2000.0]), was observed between 2003 December 26 and 2004 January 26, with more than 16 ks of exposure time. The most prominent features around the Eridanus supershell are Barnard's Loop, the I Orion O-association molecular cloud complex, the H II region surrounding λ Ori centered at $\alpha = 5^{\text{h}}32^{\text{m}}$, $\delta = +9^\circ50'$, and H α filamentary structures. To avoid excessive count rates, Barnard's Loop and the λ Ori region were excluded from the FIMS/SPEAR observation.

In a preceding paper (Ryu et al. 2006), we divided the whole Eridanus superbubble into several subregions according to its morphological structures and discussed the spectra of these subregions, focusing on H₂ molecular emissions. In the present work, a diffuse FUV image is derived from the same data set and compared with those of other wavelength bands. As our primary concern is diffuse emission, photons within 30' of the UV bright stars, identified from the Tycho-2 catalog (Wright et al. 2003), were removed from the data set to minimize stellar contamination. A total of 3.0×10^5 out of 8.8×10^5 detected photons were considered for the analysis.

After identifying and removing the stars, we obtained the diffuse image by binning the photons into 5' pixels. The photon counts were weighted by the wavelength-dependent effective area and divided by the exposure time to scale the image to the intensity level in continuum units (photons $\text{s}^{-1} \text{sr}^{-1} \text{Å}^{-1}$, hereafter CU). In deriving the diffuse emission map, only the photons from the “L channel” were considered. Those from the “S channel” were not included in the analysis due to the appearance of strong geocoronal lines, especially those of the Lyman series of hydrogen atoms. The blank spots caused by the removal of UV-bright stars were filled in the final map with the average intensity of the neighboring pixels within 3° from the spots.

3. DIFFUSE EMISSION MAPS

The resulting FUV diffuse emission image is shown in Figure 1a (Plate 1), and the H α , dust extinction, and soft X-ray maps are presented in Figures 1b, 1c, and 1d (Plate 1), respectively.

¹ Satellite Technology Research Center, Korea Advanced Institute of Science and Technology, 305-701 Daejeon, Korea; ksyu@satrec.kaist.ac.kr

² Department of Physics, Korea Advanced Institute of Science and Technology, 305-701 Daejeon, Korea.

³ Korea Astronomy and Space Science Institute, 305-348 Daejeon, Korea.

⁴ Space Sciences Laboratory, University of California, Berkeley, CA 94720.

The $H\alpha$ map, scaled in units of rayleighs, was extracted from the $H\alpha$ sky survey data reported by Reynolds et al. (1998). The dust extinction $[E(B - V)]$ map was obtained from the Galactic reddening map of Schlegel et al. (1998), which was derived from infrared observation. Finally, the soft X-ray emission map was retrieved from the *ROSAT* X-ray all-sky data (Snowden et al. 1995b) and plotted in units of 10^{-6} counts s^{-1} . In the soft X-ray map, the feature appearing as a black band, spanning from $(\alpha = 3^h30^m, \delta = -20^\circ)$ to $(\alpha = 3^h00^m, \delta = 0^\circ)$, is the region where there was no instrumental exposure. We selected six subregions based on multispectral emission features, with particular emphasis on the $H\alpha$ map in Figure 1*b*. Regions 1 and 2 correspond to the $H\alpha$ filamentary structures shown in Figure 1*b*. The cavities that are surrounded by these filaments were designated as regions 3, 4, and 5. Region 6 is a dust cloud that appears in the dust extinction map.

First, it is clearly noticeable that the features seen in the FUV diffuse emission are quite similar to those seen in the $H\alpha$ emission and the dust extinction maps. The most conspicuous features in the $H\alpha$ emission map are filamentary structures elongated along $\alpha = 4^h$ (arc A; region 1) and $\alpha = 4^h20^m$ (arc B; region 2). The main source of the $H\alpha$ emission is believed to be from recombination of hydrogen atoms ionized by strong UV light of early-type stars, probably located in the I Orion OB association. Hence, the $H\alpha$ filamentary structures seen in Figure 1*b* may be a region of high H I density, enveloping low-density regions (cavities 3, 4, and 5) with strong radiation fields.

However, the FUV diffuse emission map does not show as distinct boundaries as its $H\alpha$ counterpart. This is likely due to the source from which the FUV diffuse emission originates, although the limited exposure time of FUV observation may also contribute in part. As the FUV emission features closely follow those in the dust extinction map, we believe most of the FUV emission originates from scattering of star light off dust. Hence, the fuzzy boundaries in the FUV map may suggest that the dust scattering takes place in a wider region as compared to that of the ionization of the hydrogen atoms, which triggers the $H\alpha$ emission.

The FUV diffuse emission in the Eridanus superbubble region is composed of dust continuum scattering, H_2 fluorescent emission, and emission lines, including those from C IV. While these three components were not separated in extracting the present map, contributions other than that from the dust scattering are small, implying that the FUV diffuse emission map essentially represents the distribution of the dust-scattered UV photons. The ratios of these components are $\sim 200 : 30 : 1$ for the scattered continuum, the H_2 fluorescence, and the C IV line emission, respectively, as can be derived from the entire L channel spectra, shown in Figure 2 of Ryu et al. (2006). The diffuse background radiation, originating from the region in front of or behind the Eridanus region, may contribute to the estimated intensity of the dust-scattered FUV continuum. However, this FUV diffuse background is expected to be less than 500 CU, based on a spectrum analysis of the region outside arc B, corresponding to region 6 in Ryu et al. (2006), where all the emissions of various spectral bands are minimal. Moreover, since H_2 fluorescent emissions are still seen in this region, the continuum emissions are likely to also contain scattering by dust grains in which H_2 molecules are formed, implying that the FUV background emission level can be even lower than 500 CU.

Regions 3, 4, and 5 are commonly characterized as cavities formed by energetic phenomena such as stellar winds and su-

pernova explosions associated with the young, high-mass stars of the Orion OB association. Figure 1*d* confirms that these regions coincide with the bright regions in soft X-ray. A close examination of Figure 1*d* reveals that, while regions 4 and 5 are confined by region 2 (arc B), region 3 is bounded by region 1 (arc A). The low-intensity region between region 3 and region 5, including region 1 and its surrounding neighbor, shows clear anticorrelation with the bright triangular region of the dust extinction map in Figure 1*c*. It is also seen that region 3 is bounded from below by the dust cloud seen on the lower left corner of Figure 1*c*, where its soft X-ray counterpart is less bright. Hence, all the cavity regions 3, 4, and 5 are mostly devoid of dust. On the other hand, diffuse FUV emission is relatively bright in region 3 while it is dark in regions 4 and 5. These morphologies suggest that the cavity region 3 is associated with the molecular cloud seen as the bright regions in Figure 1*c* as well as arc A, while cavities 4 and 5 and arc B are not part of this structure.

The dust extinction feature (region 6) located at $(\alpha \sim 4^h40^m, \delta \sim -15^\circ)$ coincides with L1642, previously identified by Magnani et al. (1985). As it does not show any special correlation feature in the diffuse FUV map, the dust cloud may not be spatially related to the Eridanus superbubble. The region appears dark in the $H\alpha$ map as well as in the soft X-ray map.

4. DISCUSSION

To further investigate the relationships among the multi-wavelength observations on the $H\alpha$ shells, spectral scatter plots of the FUV diffuse emission are shown against the dust extinction and the soft X-ray intensity in Figure 2. Also shown are similar plots for region 6 (L1642). In each plot, the $H\alpha$ emission intensity at the sampling point is represented according to the color code shown at the bottom of Figure 2. The sampling points are HEALPix (Górski et al. 2005) projection cells with $N_{\text{side}} = 256$, corresponding to $\theta_{\text{pix}} = 13.7'$, which is somewhat larger than the FIMS/SPEAR spatial resolution.

Again, the spectral features of regions 1 and 2, corresponding to arcs A and B, respectively, are markedly different. For example, Figure 2*a* shows that in region 1, the FUV intensity increases with the increase in dust extinction until $E(B - V) = 0.25$, above which it no longer increases, but rather decreases likely due to strong extinction. The $H\alpha$ intensity tends to decrease with increased FUV intensity in the region where FUV intensity is proportional to the dust extinction. Figure 2*b* shows that the soft X-ray is inversely proportional to the FUV intensity in this region while the $H\alpha$ intensity increases with the increase in the intensity of soft X-ray. Hence, in region 1 the FUV intensity is proportional to the amount of dust extinction and inversely proportional to the $H\alpha$ and the soft X-ray intensities. Conversely, both the FUV intensity and the dust extinction are minimum in region 2, with the FUV intensity around 1000 CU and the $E(B - V)$ values lower than 0.1. Meanwhile, the intensity of the soft X-ray is as high as that of region 1, but shows no apparent relationship with the FUV intensity. These distinct spectral features of region 1 and region 2 suggest that arcs A and B have remarkably different physical origins. Although both $H\alpha$ filamentary structures are considered to be interstellar shocks, arc A appears to be mostly comprised of molecular and dust components, harboring large scattered diffuse FUV emissions, while arc B, which originates from atomic species, has considerably lower diffuse FUV emission and dust extinction values compared to those of arc A.

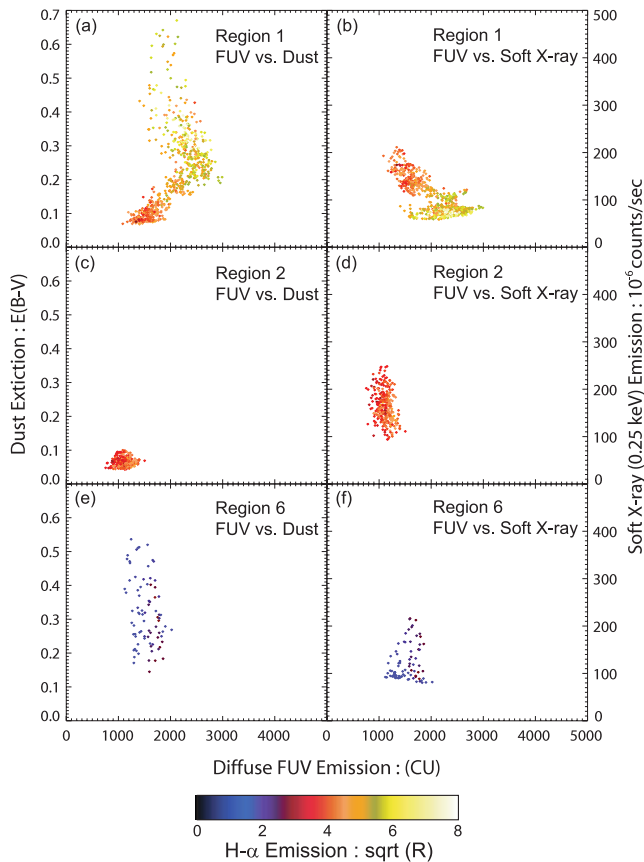


FIG. 2.—Scatter plots of the multiwavelength spectral features for the two arcs, A and B, and L1642: (a) dust extinction vs. diffuse FUV emission for region 1 (arc A), (b) soft X-ray emission vs. diffuse FUV emission for region 1 (arc A), (c) dust extinction vs. diffuse FUV emission for region 2 (arc B), (d) soft X-ray emission vs. diffuse FUV emission for region 2 (arc B), (e) dust extinction vs. diffuse FUV emission for region 6 (L1642), (f) soft X-ray emission vs. diffuse FUV emission for region 6 (L1642). The color code for the $H\alpha$ emission is shown at the bottom.

Figure 2e shows that dust extinction is strong in region 6 and the FUV intensity decreases with the increase in dust extinction. In Figure 2f, it is seen that the soft X-ray is weak and is proportional to the FUV intensity. These features suggest that L1642, being located somewhere along the line of sight, blocks the FUV emission and the soft X-rays originating behind the Eridanus region from reaching the Earth.

It was previously suggested that these arcs are spatially unrelated and likely part of two different individual shell complexes that are being viewed along the same line of sight (Boumis et al. 2001; Welsh et al. 2005). Our observations and analysis agree with these results in that arc A, surrounding region 3, is the edge of a shell that is different from the shell bounded by arc B, surrounding regions 4 and 5. Based on recent observations, the old picture regarding the geometry of the Eridanus region (Reynolds & Ogden 1979) should be modified. We suggest a new interpretation on the geometry of the region in Figure 3. As shown in the figure, arcs A and B are parts of a complex of individual shells viewed along the same line of sight at different distances (arc A, >500 pc; arc B, ~ 150 pc). Arc A is thought to be expanding through molecular clouds. The molecular cloud L1642, one of the major features in the region, is believed to be located between the Eridanus region

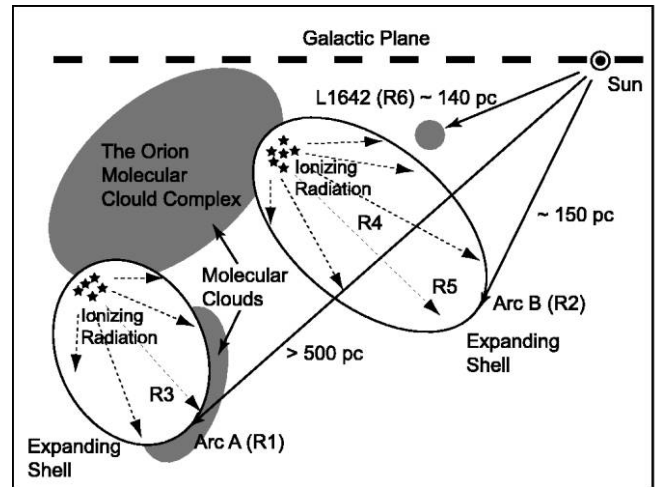


FIG. 3.—Schematic cross-sectional view of the Eridanus region. Arcs A and B are part of a complex of individual shells viewed along the same line of sight but at different distances.

and the Sun. Both shells appear to have originated from the Orion molecular cloud complex.

Hence, the present analysis suggests that arcs A and B and L1642 are all independent features. While the two arcs were once viewed as being part of a single structure (Reynolds & Ogden 1979), it was recently argued that these arcs are spatially unrelated and likely part of two different individual shell complexes that are being viewed along the same line of sight (Boumis et al. 2001; Welsh et al. 2005). Our observations agree with the latter view that arc A, surrounding region 3, is the edge of a shell that is not related to the shell bounded by arc B that surrounds regions 4 and 5. A schematic cross-sectional view of the Eridanus region is shown in Figure 3, where the distances to major features are indicated based on previous observations: arc A > 500 pc (Welsh et al. 2005), arc B ~ 150 pc (Boumis et al. 2001), and L1642 ~ 140 pc (Russeil et al. 2003).

5. SUMMARY

We have presented the first diffuse FUV emission map of the Eridanus superbubble region. The emission map of this interesting superbubble essentially represents the distribution of dust-scattered FUV photons, as other contributions including the diffuse FUV background are believed to be very small. While the $H\alpha$ map shows sharp boundaries, the FUV diffuse emission features are broader, implying that the involved dust scattering takes place in a much wider region than the photoionization that causes $H\alpha$ emission. Spectral examination revealed that one of the distinct arcs in $H\alpha$ (arc A) is mostly associated with molecular and dust components while the other (arc B) is characterized by atomic origins. The current observations confirm the earlier view that arcs A and B are part of a complex of individual shells viewed along the same line of sight but at different distances (Welsh et al. 2005).

FIMS/SPEAR is a joint project of KAIST and KASI (Korea) and UC Berkeley (USA), funded by the Korea MOST and NASA grant NAG5-5355. This research was supported by SaTReC research program.

REFERENCES

- Boumis, P., et al. 2001, MNRAS, 320, 61
Edelstein, J., et al. 2006a, ApJ, 644, L153
———. 2006b, ApJ, 644, L159
Górski, K. M., Hivon, E., Banday, A. J., Wandelt, B. D., Hansen, F. K., Reinecke, M., & Bartelmann, M. 2005, ApJ, 622, 759
Heiles, C. 1976, ApJ, 208, L137
Kregenow, J., et al. 2006, ApJ, 644, L167
Magnani, L., Blitz, L., & Mundy, L. 1985, ApJ, 295, 402
Murthy, J., Im, M., Henry, R. C., & Holberg, J. B. 1993, ApJ, 419, 739
Narayan, S., Shulman, S., Friedman, H., & Fritz, G. 1976, ApJ, 208, 718
Reynolds, R. J., & Ogden, P. M. 1979, ApJ, 229, 942
Reynolds, R. J., Tufte, S. L., Haffner, L. M., Jaehnig, K., & Percival, J. W. 1998, Publ. Astron. Soc. Australia, 15, 14
Russeil, D., Juvela, M., Mattila, K., & Paatero, P. 2003, A&A, 409, 135
Ryu, K., et al. 2006, ApJ, 644, L185
Schlegel, D. J., Finkbeiner, D. P., & Davis, M. 1998, ApJ, 500, 525
Snowden, S. L., Burrows, D. N., Sanders, W. T., Aschenbach, B., & Pfeffermann, E. 1995a, ApJ, 439, 399
Snowden, S. L., et al. 1995b, ApJ, 454, 643
Welsh, B. Y., Sallmen, S., & Jelinsky, S. 2005, A&A, 440, 547
Williamson, F. O., Sanders, W. T., Kraushaar, W. L., McCammon, D., Boriken, R., & Bunner, A. N. 1974, ApJ, 193, L133
Wright, C. O., Egan, M. P., Kraemer, K. E., & Price, S. D. 2003, AJ, 125, 359

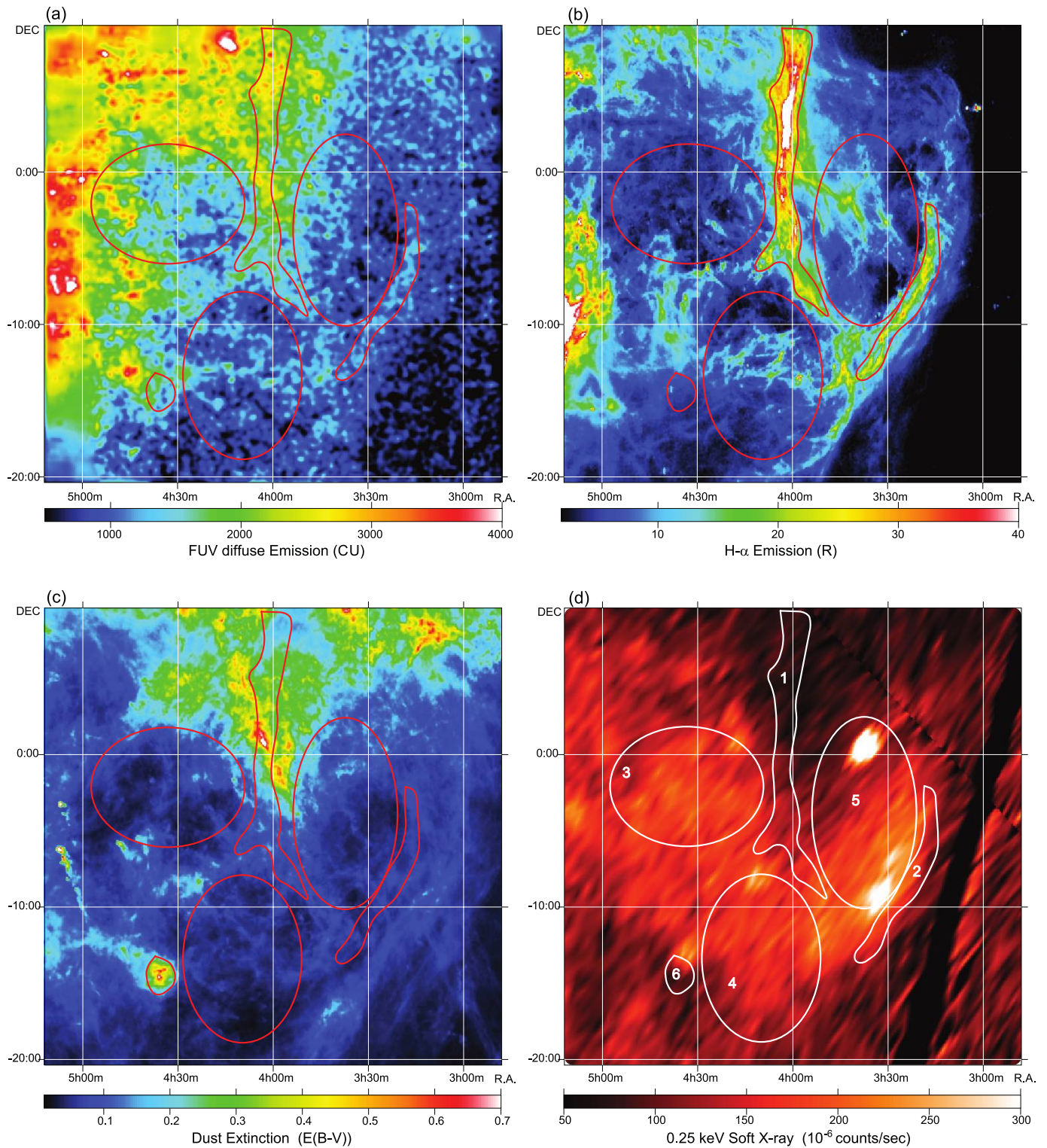


FIG. 1.—Emission maps of the Eridanus superbubble in various wavelength bands: (a) diffuse FUV emission, (b) H α emission, (c) dust extinction, and (d) 0.25 keV soft X-ray emission.